Applied Physics Letters ARTICLE pubs.aip.org/aip/apl

Physical origin of enhanced electrical conduction in aluminum-graphene composites

Cite as: Appl. Phys. Lett. **124**, 091902 (2024); doi: 10.1063/5.0195967
Submitted: 4 January 2024 · Accepted: 5 February 2024 ·
Published Online: 26 February 2024

K. Nepal,[1] C. Ugwumadu,[1] K. N. Subedi,[2] K. Kappagantula,[3] and D. A. Drabold[1,a)]

AFFILIATIONS

[1]Department of Physics and Astronomy, Nanoscale and Quantum Phenomena Institute (NQPI), Ohio University, Athens, Ohio 45701, USA
[2]Theoretical Division, Los Alamos National Laboratory, Los Alamos, New Mexico 87545, USA
[3]Pacific Northwest National Laboratory, Richland, Washington 99352, USA

[a)]Author to whom correspondence should be addressed: drabold@ohio.edu

ABSTRACT

The electronic and transport properties of aluminum-graphene composite materials were investigated using the *ab initio* plane wave density functional theory. The interfacial structure is reported for several configurations. In some cases, the face-centered aluminum (111) surface relaxes in a nearly ideal registry with graphene, resulting in a remarkably continuous interface structure. The Kubo–Greenwood formula and space-projected conductivity were employed to study electronic conduction in aluminum single- and double-layer graphene-aluminum composite models. The electronic density of states at the Fermi level is enhanced by the graphene for certain aluminum–graphene interfaces, thus improving electronic conductivity. In double-layer graphene composites, conductivity varies non-monotonically with temperature, showing an increase between 300 and 400 K at short aluminum-graphene distances, unlike the consistent decrease in single-layer composites.

Recent experimental research has shown that composites formed by the inclusion of single-layer or multiple layers of graphene into aluminum (Al) and copper (Cu) improve the electronic conduction properties of bulk metal. The interfacial structure of the metal-graphene composites is generally believed to form a high-energy configuration under suitable compression for specific experimental designs, such as hot-extrusion[1,2] or friction-extrusion[3] methods. This discovery holds promise for long-distance power transmission and other applications.[4–6]

Several works have provided insight into the mechanisms of enhanced conduction in Al-graphene (Al-G) and Cu-graphene (Cu-G) composites.[7–14] For example, Cao *et al.* showed that the electron concentration in both Al and carbon (C) atoms is contingent upon the orientation of the Al-G interface.[15] Wang *et al.* demonstrated that the incorporation of graphene additives induces a shift in the Fermi level of copper from *ab initio* calculations.[16] These studies suggest that the presence of graphene in aluminum and copper results in the alignment of metal grains in specific orientations and/or facilitates direct carrier transfer between graphene and metals. However, the precise mechanism by which this transport occurs and the impact of graphene on the global conductivity of these composites is still not well understood.

In a previous Letter in this journal,[17] we discussed electronic transport in copper-graphene composites by considering a single graphene layer sandwiched between two Cu (111) surfaces. We noted the enhancement of the electronic density of states near the Fermi level at short copper-graphene distances—suggesting improved electronic conductivity for the composites. This complementary study extends the analysis to aluminum-graphene composites. While experimentally extruded aluminum-graphene composites consist of multiple graphene layers, this study focuses on single and double layers of graphene in interface models, providing key details into the broader comprehension of the remarkable behavior of aluminum-graphene composites. We offer atomistic insights into structural relaxation at the aluminum–graphene interface and explore the temperature-dependent conductivity with the number of graphene layers in the composites. In what follows, models of aluminum–single-layer graphene–aluminum composites are referred to as SL, and aluminum–double-layer graphene–aluminum composite is referred to as DL. We focus the discussion on the DL models except where the contrast to SL is informative.

To create the Al-G composite models, we started with an orthorhombic cell of face-centered Al (111) that includes a stacking fault, as shown in Fig. 1(a). Al (111) terminations are known for their low surface energy and high electronic conductivity.[18,19] Single and double ("AB" stacking) graphene sheets were positioned above the aluminum fault layer to form an interface. The side view of the arrangement of the atoms in the SL and DL models is shown in Figs. 1(b) and 1(c), respectively. To represent the thermophysical phenomena typically

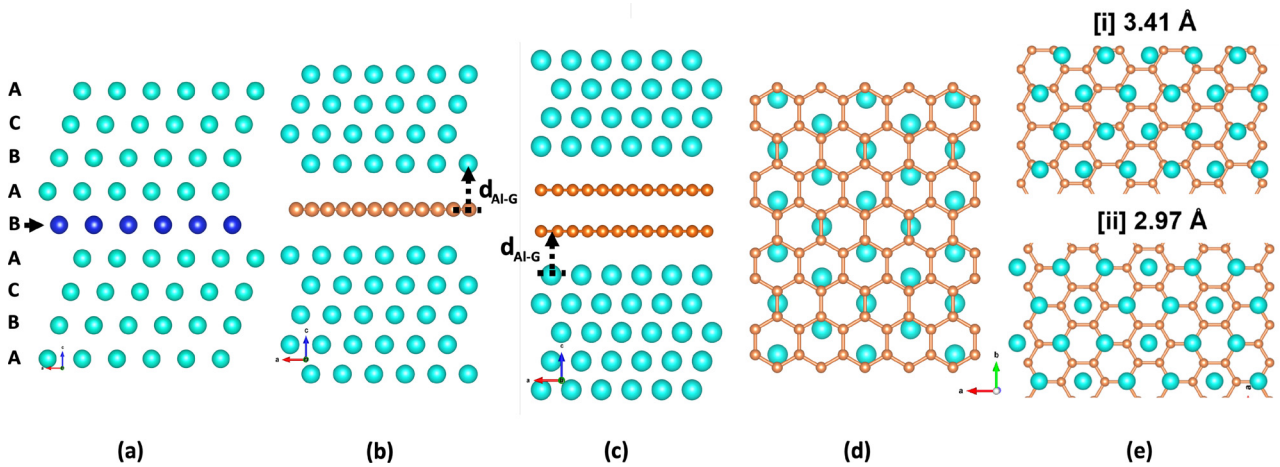

FIG. 1. (a) ABCABC... planar stacking in the Al (111) face-centered structure with a fault layer, shown by blue atoms. Representative structure of interface models with (b) single-layer and (c) double-layer graphene, where d_{Al-G} is the distance between the aluminum surface and the graphene layer. (d) Top view of the arrangement of carbon atoms in the graphene layer with Al (111) for a weakly interacting Al-graphene system with the interfacial distance of 3.48 Å (before relaxation). (e) Interface structure in composite models after the relaxation of DL composites with (i) $d_{Al-G} = 3.41$ and (ii) 2.97 Å. For $d_{Al-G} = 2.97$ Å, the optimized interface structure forms a strain-free registry between Al and C. All cyan (brown) spheres represent Al (C) atoms.

observed in solid-phase processed Al-G composites, we simulated the "compression" of the composites by reducing the Al-G distance. A similar method was employed in earlier work to study the pressure dependence of conductivity on mono-crystal copper, as well as copper–single-layer graphene–copper composite.[17,20] Next, employing the conjugate gradient algorithm within the Vienna *ab initio* simulation package (VASP),[21] an energy-optimized interface structure of the composite was attained for several constant volume simulations. The projected augmented wave (PAW) potential described the ion–election interactions, and the generalized gradient approximation (GGA) of Perdew–Burke–Ernzerhof (PBE) was implemented for the exchange-correlation functional.[22,23] The Brillouin zone was sampled using the Monkhorst-Pack[24] scheme with a $2 \times 2 \times 1$ k-point meshes. For completeness, we implemented Grimme's van der Waals (D2) correction[25] for the interfacial structure. However, post-relaxation, there was no notable disparity observed in the presence of the correction. The compression and relaxation procedures employed in this paper hope to mimic conditions commonly observed in aluminum composites that exhibit improved electrical conductivity through solid-phase processing methods. The details regarding the VASP simulation protocol and the method to create the compressed composite models are provided in the supplementary material.

Visual inspection of the composite models before any compression and structural optimization, as shown in Fig. 1(d), shows the misalignment between Al and C atoms as a honeycomb lattice of graphene (lattice constant of 2.46 Å) has a lattice mismatch of ≈ 5% with the face-centered Al (111) surface nearest-neighbor distance of 2.34 Å. However, after compression of the models followed by structural optimization (via energy minimization), there appears to be an alignment between the Al and C atoms. Figures 1(e-i) and 1(e-ii), corresponding to models with $d_{Al-G} = 3.41$ and 2.97 Å, respectively, show that the extent of atomic alignments between C and Al is dependent on the extent of the compression. The self-organized interface configuration for the compressed model ($d_{Al-G} = 2.97$ Å in this work) is one of the low energy Al-G interface structure, so-called strain-free registry.[26–28]

We computed the atom-projected electronic density of states (PDoS) for varying interfacial distance models. The PDoS for the SL and DL composite models are shown in Figs. 2(a) and 2(b), respectively. The focus is on the region near the Fermi energy (ε_f), indicated by the gray dashed lines and shifted to zero. As the distance between aluminum and graphene (Al-G distance) decreased, we observed an

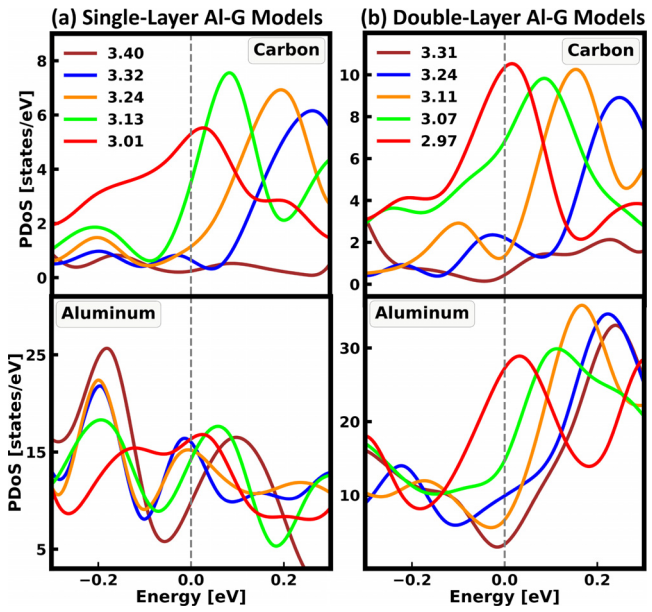

FIG. 2. Projected electron density of states (PDoS) on carbon and aluminum atoms for (a) SL and (b) DL composites. The Fermi level is shifted to zero and is shown by the gray vertical dashed line in each subplot.

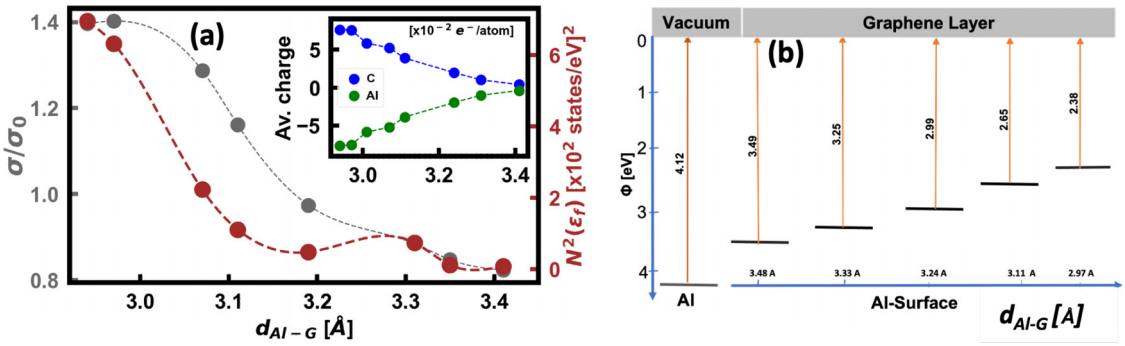

FIG. 3. (a) Conductivity for the DL model for various Al-G distances (d_{Al-G}) in the x axis. The average conductivity (σ) is represented by the gray curve, with σ_0 denoting the conductivity of the Al-matrix shown in Fig. 1(a) calculated at 300 K. The squared density of states at the Fermi level is shown in brown. In the inset, a Bader analysis[29] illustrates the average charge gain and loss for C (blue) and Al (green) atoms. (b) Estimated energy (Φ) required to remove an electron from pure Al surface and with graphene layer placed on it at different interfacial distances. Dotted lines are included in all plots as visual aids.

enhancement of the electronic density of states near the Fermi level from both carbon (TOP) and aluminum (BOTTOM) atoms. With a random phase approximation,[30–33] Mott and Davis showed that the electronic conductivity is proportional to $N^2(\varepsilon_f)$,[34] and $N(\varepsilon_f)$ is the density of states at the Fermi energy (ε_f). To explore this further, we plotted the behavior of $N^2(\varepsilon_f)$ for the compressed composite models [brown curve in Fig. 3(a)]. Indeed, $N^2(\varepsilon_f)$ roughly tracks the electronic conductivity (σ) calculated using the Kubo–Greenwood formula (KGF),[35–37] shown by gray curve in Fig. 3(a). As the Al-G distance decreases, both $N^2(\varepsilon_f)$ and electronic conductivity increase, consistent with the elementary notion that metallicity/conduction is associated with a large $N(\varepsilon_f)$. The DL composites ($d_{Al-G} = 2.97$ and 2.94 Å) exhibit approximately 40% higher conductivity relative to the aluminum matrix at 300 K. These results qualitatively agree with the results reported for copper–graphene interface.[17,38] Next, we depicted a flattening in the electrical conductivity for the compression beyond 2.97 Å, detailed below. Analogous results for the SL models can be found in Fig. S1 in the supplementary material.

To provide salient background information on the electrical conductivity, the conductivity in orthorhombic face-centered (111) aluminum was analyzed as a function of the Al–Al bond length (refer to Fig. S2). Electrical conductivity in aluminum increases with decreasing Al–Al bond length (d_{Al-Al}) until $\approx$2.76 Å. Beyond this threshold, a decrease in conductivity is observed. In DL composites with $d_{Al-G} = 2.97$ and 2.94 Å, the mean Al–Al bond length was $d_{Al-Al} = 2.76$ Å, corresponding to d_{Al-Al} with the highest electrical conductivity, as depicted in Fig. S2. Further compression in the composite resulting in $d_{Al-G} < 2.94$ Å exhibited a decrease in the electrical conductivity. This trend is consistent with observations in copper-graphene heterostructures.[17,38]

The Fermi level shifts toward higher energies with decreasing Al-G distance, allowing more electronic states to participate in conduction (see details in Table I). This behavior has been reported for graphene on copper.[16,17] We further predicted the work function of the composites for varying Al-G distances, which is shown in Fig. 3(b). The plot shows that the work function decreases with decreasing Al-G distance and hints at increasing charge transfer between interfacial graphene and aluminum atoms. These effects are quantified by estimating the average charge transfer from interfacial Al to C atoms, shown in the inset of Fig. 3(a). At the shortest interfacial distance ($d_{Al-G} = 2.97$ Å), the average transfer of electronic charge to graphene reached 0.075 electrons per atom. Enhancing charge transfer and interface bonding can be achieved through graphene doping with boron, nitrogen, and silicon, as reported in other studies.[39,40]

Next, we computed the conduction path in real space and its Al-G distance dependence. To achieve this, we employed the space-projected conductivity (SPC) method to project the electronic conductivity onto real-space grids.[41–43] The upper panel of Fig. 4 shows the isosurface plots of the transverse SPC values for DL composite models with interfacial distances of 3.41 and 2.97 Å, represented by (a) and (b) in Fig. 4, respectively. The color bar on the right indicates the magnitude of SPC values, with red (blue) indicating low (high) values. At short Al-G distances, both aluminum and graphene contribute to conduction, particularly at the Al-G interface. The SPC at short Al-G distances reveals that graphene actively participates in conduction and forms a bridge between Al atoms on opposite layers. Notably, Fig. 4 (upper panel) illustrates the formation of a continuous network of graphene sheets within the aluminum matrix, establishing a pathway for electron transport.

To further delineate the enhanced electron transport through the Al-G interface, we computed the electronic charge density near the Fermi level (see implementation examples in Refs. 44–47). By decomposing 15 bands above and below the Fermi level from the total electron charge density, we generated isosurface plots, shown in the lower panel of Fig. 4. The same models used for the SPC calculation were employed. In the model with $d_{Al-G} = 2.97$ Å, a higher degree of interaction between graphene and interfacial aluminum atoms was

TABLE I. Fermi level as a function of Al-G composites for varying aluminum–graphene interfacial distance. The first and second row corresponds to DL and SL composites, respectively.

d_{Al-G} (Å)	3.41	3.35	3.31	3.24	3.19	3.11	3.07	2.97	2.94
E_f (eV)	6.70	6.79	6.93	7.05	7.20	7.29	7.36	7.52	7.63
d_{Al-G} (Å)	3.40	3.35	3.31	3.25	3.13	3.01	2.90	2.71	
E_f (eV)	6.78	7.07	7.34	7.62	7.87	8.18	8.43	8.67	

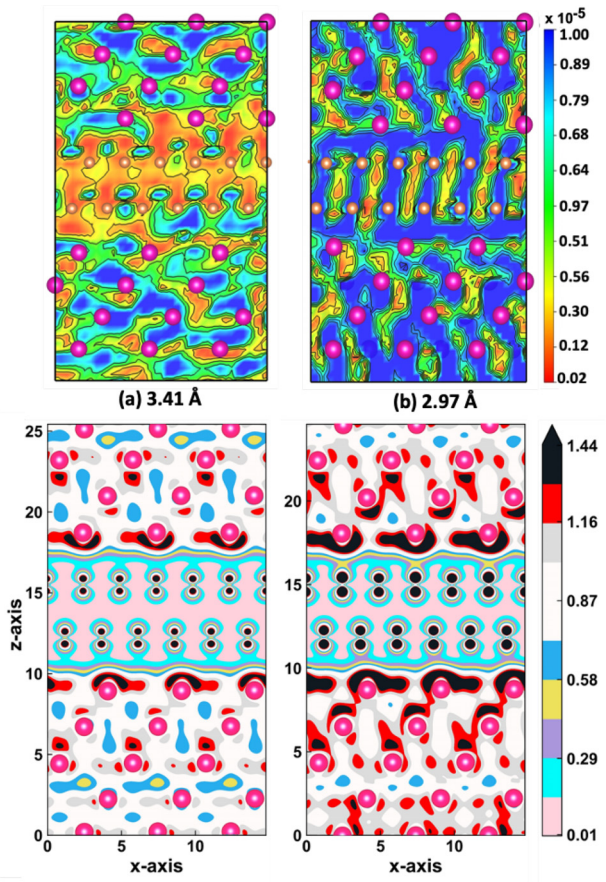

FIG. 4. (Top) Projected 2D transverse SPC (in Siemens/cm/Å^3) iso-surface plot. (Bottom) Band decomposed charge density (in e^{-}/Å^3) corresponds to 15 bands below and above the Fermi level. The charge density values were scaled by a factor of 100. The data presented are for DL models with d_{Al-G} = (a) 3.41 and (b) 2.97 Å. The pink (brown) spheres represent the Al (C) atoms in the models.

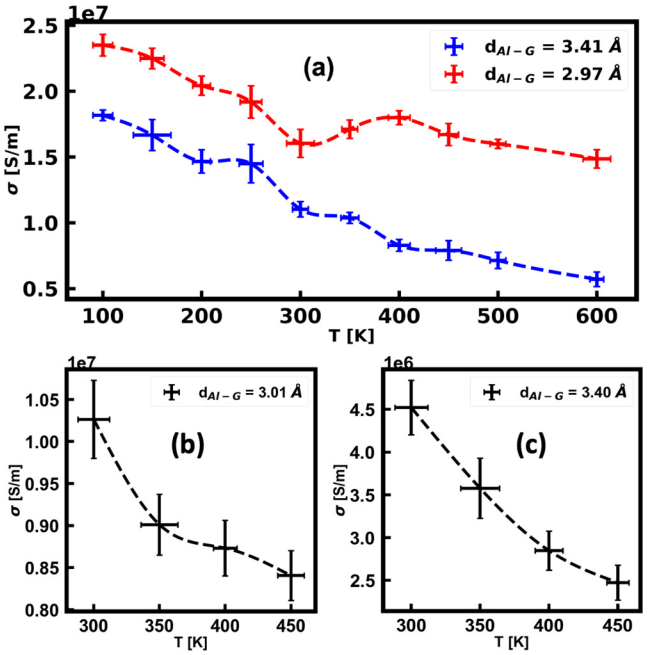

FIG. 5. (a) Average electronic conductivity plotted vs annealing temperature for DL composite models with Al-G distances of 2.97 Å (red) and 3.41 Å (blue). (b) and (c) Similar plots for SL composite models, with Al-G distances of 3.01 and 3.40 Å, respectively. Vertical bars represent the standard deviation from the mean conductivity, averaged from the last 10 snapshots taken at 50 fs intervals over 3 ps annealing. Horizontal bars represent temperature fluctuations during constant temperature annealing.

observed, indicated by the presence of black and red regions in the iso-surface plot.

Next, we investigated the temperature dependence of conductivity in the composite models. This was done by estimating the average electrical conductivity from KGF for models held at different temperatures. The procedure to calculate the temperature-dependent conductivity is discussed in the supplementary material. Figure 5 presents the average electronic conductivity, obtained from 10 uncorrelated snapshots, as a function of temperature, ranging from 100 to 600 K. Figure 5(a) shows the conductivity behavior for the DL models corresponding to two interfacial distances. The model with $d_{Al-G} = 3.41$ Å exhibits a nearly linear relationship, shown by blue plots. However, the model with short Al-G distance, $d_{Al-G} = 2.97$ Å (shown by red plots), displays local extrema at around 300 K (minima) and 400 K (maxima). This non-monotonic behavior is in accord with experimental observations of conductivity enhancement in solid-phase processed metal-graphene composites,[1,3] suggesting that this work captures, to some extent, the physics of the real material. In contrast, the extrema are not observed in the SL composite models, as shown in Figs. 5(b) and 5(c), which correspond to Al-G distances $d_{Al-G} = 3.01$ and 3.40 Å, respectively. The non-monotonic temperature dependence observed exclusively in the compressed DL composites can be attributed to two factors: (1) the active involvement of graphene layers in charge transfer at shorter Al-G distances and (2) thermally driven hopping across the inter-layer galleries between the compressed graphene double-layer.[48–51]

We show that graphene and graphene stacks enhance the electronic conductivity of Al and while a key addition to the area, it is not the full story. The graphene structures are dispersed in an unknown way throughout the metal microstructures in the experimentally synthesized bulk composites and conspire to create a globally enhanced conductivity and globally modified temperature dependence. These effects could be due to (1) reduced scattering at grain boundaries from the graphene or (2) forming a network of isolated or weakly interacting Al-G structures. Our work complements both of these imaginings. The registry between the sp^2 carbon network [see Fig. 1(e-ii)] and the Al (111) surface suggests that mechanism (1) may be a key player in conductivity enhancement, as we demonstrate that a self-organized grain boundary buffer may form at Al (111) surfaces.

In conclusion, this study provides a comprehensive atomic-level understanding of the role of graphene as an additive in aluminum grains, focusing on single- and double-graphene stack(s) in the aluminum matrix. We have demonstrated that the increased electrical conductivity observed in Al-graphene composites arises from the enhanced electronic dynamics at the Fermi level. The interaction between carbon and interfacial aluminum atoms highlights the active

role of graphene in facilitating electronic conduction. Furthermore, our study depicts the experimentally observed enhanced electrical conductivity within the temperature range of 300–400 K.

See the supplementary material for the procedures used for optimizing geometry and conducting electronic structure calculations with specific functionals and cutoffs in VASP; compression was applied, and temperature-dependent conductivity calculations were executed according to a defined protocol; and graphical presentations illustrate the electrical conductivity dependencies for aluminum single-layer composites and orthorhombic fcc aluminum on compression.

The authors gratefully acknowledge the support received from the National Science Foundation (NSF) for computational resources through XSEDE (Grant No. ACI-1548562; Allocation No. DMR-190008P) and ACCESS (Grant Nos. 2138259, 2138286, and 2138296; Allocation No. phy230007p and phy230039p). The authors also acknowledge the support received from the Department of Energy (DOE) Vehicles Technology Office Powertrain Materials Core Program. Pacific Northwest National Laboratory is operated by the Battelle Memorial Institute for the U. S. Department of Energy under Contract No. DE-AC06-76LO1830.

AUTHOR DECLARATIONS

Conflict of Interest

The authors have no conflicts to disclose.

Author Contributions

Kishor Nepal: Conceptualization (equal); Formal analysis (equal); Investigation (equal); Software (equal); Validation (equal); Visualization (equal); Writing – original draft (equal). **Chinonso Ugwumadu:** Conceptualization (equal); Formal analysis (equal); Investigation (equal); Validation (equal); Visualization (equal); Writing – review & editing (equal). **Kashi Subedi:** Formal analysis (equal); Software (equal); Validation (equal); Writing – review & editing (equal). **Keerti Kappagantula:** Conceptualization (equal); Formal analysis (equal); Funding acquisition (equal); Investigation (equal); Project administration (equal); Supervision (equal); Validation (equal); Writing – review & editing (equal). **David A. Drabold:** Conceptualization (equal); Funding acquisition (equal); Investigation (equal); Methodology (equal); Project administration (equal); Validation (equal); Writing – review & editing (equal).

DATA AVAILABILITY

The data that support the findings of this study are available from the corresponding author upon reasonable request.

REFERENCES

[1]A. Nittala, J. Smith, B. Gwalani, J. Silverstein, F. Kraft, and K. Kappagantula, "Simultaneously improved electrical and mechanical performance of hot-extruded bulk scale aluminum-graphene wires," Mater. Sci. Eng. B **293**, 116452 (2023).
[2]K. S. Kappagantula, J. A. Smith, A. K. Nittala, and F. F. Kraft, "Macro copper-graphene composites with enhanced electrical conductivity," J. Alloys Compd. **894**, 162477 (2022).
[3]B. Gwalani, X. Li, A. Nittala, W. Choi, M. Reza-E-Rabby, J. Atehortua, A. Bhattacharjee, M. Pole, J. Silverstein, M. Song, and K. Kappagantula, "Unprecedented electrical performance of friction-extruded copper-graphene composites," Mater. Des. **237**, 112555 (2023).
[4]A. K. Sharma, R. Bhandari, and C. Pinca-Bretotean, "A systematic overview on fabrication aspects and methods of aluminum metal matrix composites," Mater. Today: Proc. **45**, 4133–4138 (2021).
[5]K. Jiju, S. Gurusamy, and S. Prakash, "Study on preparation of Al-SiC metal matrix composites using powder metallurgy technique and its mechanical properties," Mater. Today: Proc. **27**, 1843–1847 (2020).
[6]X. Sauvage, E. V. Bobruk, M. Y. Murashkin, Y. Nasedkina, N. A. Enikeev, and R. Z. Valiev, "Optimization of electrical conductivity and strength combination by structure design at the nanoscale in Al-Mg-Si alloys," Acta Mater. **98**, 355 (2015).
[7]J. Tokutomi, T. Uemura, S. Sugiyama, J. Shiomi, and J. Yanagimoto, "Hot extrusion to manufacture the metal matrix composite of carbon nanotube and aluminum with excellent electrical conductivities and mechanical properties," CIRP Ann. Manuf. Technol. **64**, 257–260 (2015).
[8]F. A. Chyada, A. R. Jabur, and H. A. Alwan, "Effect addition of graphene on electrical conductivity and tensile strength for recycled electric power transmission wires," Energy Procedia **119**, 121–130 (2017).
[9]L. Brown, P. Joyce, D. Forrest, and L. Salamanca-Riba, "Physical and mechanical characterization of a nanocarbon infused aluminum-matrix composite," Mater. Perform. Charact. **3**, 65–80 (2014).
[10]A. M. Ali, M. Z. Omar, H. Hashim, M. S. Salleh, and I. F. Mohamed, "Recent development in graphene-reinforced aluminium matrix composite: A review," Rev. Adv. Mater. Sci. **60**, 801–817 (2021).
[11]X. Zhang and S. Wang, "Interfacial strengthening of graphene/aluminum composites through point defects: A first-principles study," Nanomaterials **11**, 738 (2021).
[12]D.-Y. Kim and H.-J. Choi, "Recent developments towards commercialization of metal matrix composites," Materials **13**, 2828 (2020).
[13]M. S. Ayar, P. M. George, and R. R. Patel, "Advanced research progresses in aluminium metal matrix composites: An overview," AIP Conf. Proc. **2317**, 020026 (2021).
[14]K. Nepal, C. Ugwumadu, A. Gautam, K. Kappagantula, and D. A. Drabold, "Electronic conductivity in metal-graphene composites: The role of disordered carbon structures, defects, and impurities," J. Phys. Mater. **7**, 025003 (2024).
[15]M. Cao, Y. Luo, Y. Xie, Z. Tan, G. Fan, Q. Guo, Y. Su, Z. Li, and D.-B. Xiong, "The influence of interface structure on the electrical conductivity of graphene embedded in aluminum matrix," Adv. Mater. Interfaces **6**, 1900468 (2019).
[16]W. Wang, Y. Liu, T. Wang, K. Sheng, and B. Yu, "Graphene/Cu (111) interface study: The density functional theory calculations," in *International Conference on Electronics, Communications and Control (ICECC)* (IEEE, 2011), pp. 265–268.
[17]K. N. Subedi, K. Nepal, C. Ugwumadu, K. Kappagantula, and D. A. Drabold, "Electronic transport in copper-graphene composites," Appl. Phys. Lett. **122**, 031903 (2023).
[18]J.-M. Zhang, F. Ma, and K.-W. Xu, "Calculation of the surface energy of FCC metals with modified embedded-atom method," Appl. Surf. Sci. **229**, 34–42 (2004).
[19]Y. Wang, M. Li, P. Peng, H. Gao, J. Wang, and B. Sun, "Preferred orientation at the Al/graphene interface: First-principles calculations and experimental observation," J. Alloys Compd. **900**, 163304 (2022).
[20]N. A. Lanzillo, J. B. Thomas, B. Watson, M. Washington, and S. K. Nayak, "Pressure-enabled phonon engineering in metals," Proc. Natl. Acad. Sci. U. S. A. **111**, 8712–8716 (2014).
[21]G. Kresse and J. Hafner, "*Ab initio* molecular dynamics for liquid metals," Phys. Rev. B **47**, 558–561 (1993).
[22]P. E. Blöchl, "Projector augmented-wave method," Phys. Rev. B **50**, 17953–17979 (1994).
[23]J. P. Perdew, K. Burke, and M. Ernzerhof, "Generalized gradient approximation made simple [Phys. Rev. Lett. 77, 3865 (1996)]," Phys. Rev. Lett. **78**, 1396–1396 (1997).
[24]H. J. Monkhorst and J. D. Pack, "Special points for Brillouin-zone integrations," Phys. Rev. B **13**, 5188 (1976).
[25]S. Grimme, "Semiempirical GGA-type density functional constructed with a long-range dispersion correction," J. Comput. Chem. **27**, 1787–1799 (2006).

[26]Y. Qi, L. G. Hector, N. Ooi, and J. B. Adams, "A first principles study of adhesion and adhesive transfer at Al(111)/graphite(0001)," Surf. Sci. **581**, 155–168 (2005).
[27]W. Lee, S. Jang, M. J. Kim, and J. M. Myoung, "Interfacial interactions and dispersion relations in carbon-aluminium nanocomposite systems," Nanotechnology **19**, 285701 (2008).
[28]Y. Qi and L. G. Hector, "Adhesion and adhesive transfer at aluminum/diamond interfaces: A first-principles study," Phys. Rev. B **69**, 235401 (2004).
[29]W. Tang, E. Sanville, and G. Henkelman, "A grid-based Bader analysis algorithm without lattice bias," J. Phys.: Condens. Matter **21**, 084204 (2009).
[30]N. K. Hindley, "Random phase model of amorphous semiconductors I. Transport and optical properties," J. Non-Cryst. Solids **5**, 17–30 (1970).
[31]N. K. Hindley, "Random phase model of amorphous semiconductors II. Hot electrons," J. Non-Cryst. Solids **5**, 31–40 (1970).
[32]L. Friedman and N. F. Mott, "The hall effect near the metal-insulator transition," in *Sir Nevill Mott – 65 Years in Physics* (World Scientific, 1995), pp. 529–534.
[33]L. Friedman, "Hall conductivity of amorphous semiconductors in the random phase model," J. Non-Cryst. Solids **6**, 329–341 (1971).
[34]N. F. Mott and E. A. Davis, *Electronic Processes in Non-Crystalline Materials*, 2nd ed. (Clarendon/Oxford University Press, Oxford, New York, 1979), Chap. 2, pp. 6–58.
[35]R. Kubo, "Statistical-mechanical theory of irreversible processes. I. General theory and simple applications to magnetic and conduction problems," J. Phys. Soc. Jpn. **12**, 570–586 (1957).
[36]D. A. Greenwood, "The Boltzmann equation in the theory of electrical conduction in metals," Proc. Phys. Soc. **71**, 585–596 (1958).
[37]L. L. Moseley and T. Lukes, "A simplified derivation of the Kubo-Greenwood formula," Am. J. Phys. **46**, 676–677 (1978).
[38]A. Samal, A. K. Kushwaha, D. Das, M. R. Sahoo, N. A. Lanzillo, and S. K. Nayak, "Thermal and electrical conductivity of copper-graphene heterosystem: An effect of strain and thickness," Adv. Eng. Mater. **25**, 2201192 (2023).
[39]P. Liu, J. Xie, A. Wang, D. Ma, and Z. Mao, "First-principles prediction of enhancing graphene/Al interface bonding strength by graphene doping strategy," Appl. Surf. Sci. **517**, 146040 (2020).
[40]Y. Mei, B. Ju, W. Yang, Z. Xiu, B. Zhao, and G. Wu, "First-principles prediction of enhancing graphene-Al interface bonding by Si-doping," Appl. Compos. Mater. **28**, 1845 (2021).
[41]K. N. Subedi, K. Kappagantula, F. Kraft, A. Nittala, and D. A. Drabold, "Electrical conduction processes in aluminum: Defects and phonons," Phys. Rev. B **105**, 104114 (2022).
[42]K. N. Subedi, K. Prasai, M. N. Kozicki, and D. A. Drabold, "Structural origins of electronic conduction in amorphous copper-doped alumina," Phys. Rev. Mater. **3**, 065605 (2019).
[43]K. N. Subedi, K. Prasai, and D. A. Drabold, "Space-projected conductivity and spectral properties of the conduction matrix," Phys. Status Solidi B **258**, 2000438 (2020).
[44]C. Ugwumadu, K. Nepal, R. Thapa, Y. Lee, Y. Al Majali, J. Trembly, and D. Drabold, "Simulation of multi-shell fullerenes using machine-learning Gaussian approximation potential," Carbon Trends **10**, 100239 (2023).
[45]C. Ugwumadu, R. Thapa, Y. Al-Majali, J. Trembly, and D. A. Drabold, "Formation of amorphous carbon multi-walled nanotubes from random initial configurations," Phys. Status Solidi B **260**, 2200527 (2023).
[46]C. Ugwumadu, R. Thapa, K. Nepal, and D. A. Drabold, "Atomistic nature of amorphous graphite," Phys. Chem. Glasses **64**, 16–22 (2023).
[47]R. Thapa, C. Ugwumadu, K. Nepal, J. Trembly, and D. A. Drabold, "*Ab initio* simulation of amorphous graphite," Phys. Rev. Lett. **128**, 236402 (2022).
[48]S. Ono, "*C*-axis resistivity of graphite in connection with stacking faults," J. Phys. Soc. Jpn. **40**, 498–504 (1976).
[49]N. Iwashita, H. Imagawa, and W. Nishiumi, "Variation of temperature dependence of electrical resistivity with crystal structure of artificial graphite products," Carbon **61**, 602–608 (2013).
[50]S. Bapat, "Thermal conductivity and electrical resistivity of two types of ATJ-S graphite to 3500° K," Carbon **11**, 511–514 (1973).
[51]K. Matsubara, K. Sugihara, and T. Tsuzuku, "Electrical resistance in the *c* direction of graphite," Phys. Rev. B **41**, 969–974 (1990).